Delayed Advective Oscillation of the Atlantic Thermohaline Circulation

Sang-Ki Lee[1,2] and Chunzai Wang[2]

[1]Cooperative Institute for Marine and Atmospheric Studies, University of Miami, Miami FL

[2]Atlantic Oceanographic and Meteorological Laboratory, NOAA, Miami FL

Submitted to Journal of Climate as a Note

July 2009

Corresponding author address: Dr. Sang-Ki Lee, NOAA/AOML, 4301 Rickenbacker Causeway, Miami, FL 33149, USA. E-mail: Sang-Ki.Lee@noaa.gov.

ABSTRACT

A simple dynamic model is proposed to illustrate the multidecadal oscillation of the Atlantic thermohaline circulation. The proposed oscillation relies on alternating actions of positive and negative feedbacks, which are operated by a slow adjustment of the baroclinic ocean circulation and the associated delayed advection in response to a meridional density gradient. For a sufficiently long delay time, the solution becomes unstable and oscillates with a period of about twice the delay. For a shorter delay time, large amplitude of weather noise can sustain an active delayed advective oscillation of an otherwise stable damped oscillation.

1. Introduction

The objective of this note is to propose a simple dynamic model for the multidecadal oscillation of the Atlantic thermohaline circulation, also known as the Atlantic Meridional Overturning Oscillation (AMOC), simulated in general circulation models (e.g., Delworth et al. 1993; Knight et al. 2005). The proposed oscillation relies on alternating actions of positive and negative feedbacks, which are operated by a delayed advection of meridional density gradient. The key element of the delayed density advection originates from a slow adjustment of the baroclinic ocean circulation in response to a meridional density gradient (Killworth, 1985). Here, a four-box model is used to illustrate the delayed advective oscillator.

2. The four-box model

The North Atlantic Ocean is simplified with four boxes with two-layer structures in the high- and low-latitudes, as shown in Figure 1. The meridional density gradient is always positive, thus the volume transport must be northward in the upper layer and southward in the lower layer. Conservation of mass dictates that the volume transport at the mid-depth is downward in the high-latitude and upward in the low-latitude. Therefore, volume integration of the density conservation equation for each box yields

$$\frac{d\rho_1}{dt} = V(\rho_4 - \rho_1) - q - r\rho_1^3 - \frac{k_v}{H^2}(\rho_1 - \rho_4) + F_1, \tag{1}$$

$$\frac{d\rho_2}{dt} = V(\rho_1 - \rho_2) + q - r\rho_2^3 - \frac{k_v}{H^2}(\rho_2 - \rho_3) + F_2, \tag{2}$$

$$\frac{d\rho_3}{dt} = V(\rho_2 - \rho_3) - r\rho_3^3 + \frac{k_v}{H^2}(\rho_2 - \rho_3) + F_3, \tag{3}$$

$$\frac{d\rho_4}{dt} = V(\rho_3 - \rho_4) - r\rho_4^3 + \frac{k_v}{H^2}(\rho_1 - \rho_4) + F_4, \tag{4}$$

where ρ_1, ρ_2, ρ_3 and ρ_4 are densities of the upper low-latitude box, upper high-latitude box, lower high-latitude box, and lower low-latitude box, respectively; V is the volume transport per unit volume in response to the meridional density gradient; q is density flux into the upper high-latitude box (or out of the upper low-latitude box); r is a damping coefficient; k_v is a vertical diffusion coefficient; H is the model ocean depth divided by 2; F_1, F_2, F_3 and F_4 represent other forcing terms such as horizontal diffusion and convective mixing.

Now, a separate equation for V is required to solve the equations (1)-(4). Using the geostrophic balance and hydrostatic relation, the zonal baroclinic (i.e., upper - lower layer) velocity in the mid-latitude corresponding to the north-south density gradient can be written as

$$\hat{u} = \frac{gH}{\rho_o f_o L_y}\left(\rho_{23} - \rho_{14}\right), \tag{5}$$

where g is the gravitational acceleration; ρ_o is a reference density; f_o is the planetary vorticity in the mid-latitude; L_y is the meridional length of the model domain divided by 2; $\rho_{14} = (\rho_1 + \rho_4)/2$, and $\rho_{23} = (\rho_2 + \rho_3)/2$. See Killworth (1985) for a detailed derivation of the equation (5). As discussed in Killworth (1985), the baroclinic meridional motions establish after the adjustment time, which depends on the basin-crossing time of long baroclinic Rossby wave. Therefore, in this study, the meridional volume transport (per unit volume) is represented by using the equation (5) with a time delay:

$$V = \alpha \frac{gH}{2\rho_o f_o L_y^2}\left[\rho_{23}\left(t-\delta\right) - \rho_{14}\left(t-\delta\right)\right], \tag{6}$$

where α is a constant on the order of 1; and δ is the time delay, which is about the basin-crossing time of long Rossby wave.

Scaling time by $2f_oL_y^2/(g'H)$, ρ by $\sqrt{g'H/(2rf_oL_y^2)}$, and q by $\sqrt{r^{-1}[g'H/(2f_oL_y^2)]^3}$, the following non-dimensional equations can be derived:

$$\frac{d\rho_1}{dt} = \alpha[\rho_{23}(t-\delta) - \rho_{14}(t-\delta)](\rho_4 - \rho_1) - q - \rho_1^3 - k_o(\rho_1 - \rho_4) + F_1, \tag{7}$$

$$\frac{d\rho_2}{dt} = \alpha[\rho_{23}(t-\delta) - \rho_{14}(t-\delta)](\rho_1 - \rho_2) + q - \rho_2^3 - k_o(\rho_2 - \rho_3) + F_2, \tag{8}$$

$$\frac{d\rho_3}{dt} = \alpha[\rho_{23}(t-\delta) - \rho_{14}(t-\delta)](\rho_2 - \rho_3) - \rho_3^3 + k_o(\rho_2 - \rho_3) + F_3, \tag{9}$$

$$\frac{d\rho_4}{dt} = \alpha[\rho_{23}(t-\delta) - \rho_{14}(t-\delta)](\rho_3 - \rho_4) - \rho_4^3 + k_o(\rho_1 - \rho_4) + F_4, \tag{10}$$

where the non-dimensional vertical diffusivity $k_o = 2k_v f_o L_y^2/(g'H^3)$.

3. The one-equation model

In order to gain some insights on the behavior of the nonlinear system of equations (7)-(10), a simplified one-equation model is derived and evaluated here. Specifically, it is assumed that ρ_2, ρ_3, and ρ_4 are close to each other enough to be represented as a single variable $\rho_2^* = (\rho_2 + \rho_3 + \rho_4)/3$. This is not an unreasonable assumption because the convective process maintains ρ_3 as close to ρ_2, and the advective flux from the box-3 to box-4 also keeps ρ_4 close to ρ_3 for a sufficiently small value of k_o. Then, the density budget equations (7)-(11) can be simplified to a single equation:

$$\frac{d\hat{\rho}}{dt} = -\frac{2}{3}\alpha\hat{\rho}(t-\delta)\hat{\rho} + \frac{4}{3}q - \frac{4}{3}k_o\hat{\rho} - \hat{\rho}^3, \tag{11}$$

where $\hat{\rho} = \rho_2^* - \rho_1$, and the nonlinear dissipation term is slightly modified from its original form. If $\delta = 0$, this equation has a positive steady state solution. By neglecting the nonlinear dissipation term for the sake of illustration, the positive steady solution $\hat{\rho}_o$ is

$$\hat{\rho}_o = \frac{(-k_o + \sqrt{k_o^2 + 2\alpha q})}{\alpha}. \tag{12}$$

The linear stability of $\hat{\rho}_o$ in the equation (11) can be studied by replacing $\hat{\rho}(t)$ in (11) with the sum of the stationary solution $\hat{\rho}_o$ and the perturbation $\hat{\rho}'(t)$. Retaining only the linear terms, the perturbation equation can be written as

$$\frac{d\hat{\rho}'}{dt} = -\frac{2}{3}\left(\alpha\hat{\rho}_o + 2k_o + 4.5\hat{\rho}_o\right)\hat{\rho}' - \frac{2}{3}\alpha\hat{\rho}_o\hat{\rho}'(t-\delta). \tag{13}$$

Seeking solutions of the form $\hat{\rho}' \propto \exp(\sigma t)$ with $\sigma = \sigma_r + i\sigma_i$, the following equations can be derived:

$$\sigma_r = -\frac{2}{3}(\alpha\hat{\rho}_o + 2k_o + 4.5\hat{\rho}_o^2) - \frac{2}{3}\alpha\hat{\rho}_o e^{-\sigma_r\delta}\cos(\sigma_i\delta), \tag{14}$$

$$\sigma_i = \frac{2}{3}\alpha\hat{\rho}_o e^{-\sigma_r\delta}\sin(\sigma_i\delta). \tag{15}$$

If σ_r is positive, the first term in the RHS of (14) is always larger than the second term, thus the equation (14) cannot be satisfied. Therefore, σ_r is negative regardless of σ_i. This means that the simplified density budget equation (11) is always stable around $\hat{\rho}_o$. However, it is shown in the next section that the nonlinear system of equations (7)-(10) is unstable for a sufficiently large value of δ. This suggests that the density budgets in the lower layers (box-3 and -4) must be fully incorporated to resolve the delayed advective oscillation of the AMOC.

4. Numerical solutions

The behavior of the nonlinear equations (7) - (10) is explored numerically using a fourth-order Runge-Kutta scheme. When the upper layer is heavier than the layer below, the convective mixing is achieved by completely mixing the two layers. Horizontal diffusion is turned off for simplicity. Figure 2 shows three model solutions for δ = 0, 7 and 20, when α, q and k_o are set to 2.0, 0.1 and 0.2, respectively. The dashed lines are the statistical equilibrium values. For small values of δ, the solution achieves a stable state. For a larger value of δ, on the other hand, the solution oscillates with a period of about twice the delay.

Obviously, at issue is why the solution oscillates when the advective delay is sufficiently long. To answer this question, the equation for the density difference between the high-latitude boxes and low-latitude boxes is diagnosed here:

$$\frac{d(\rho_{23}-\rho_{14})}{dt} = \alpha\left[\rho_{23}(t-\delta)-\rho_{14}(t-\delta)\right](\rho_1-\rho_3)+q-\frac{1}{2}\left[\left(\rho_2^3+\rho_3^3\right)-\left(\rho_1^3+\rho_4^3\right)\right]. \qquad (16)$$

Figure 3 shows [ρ_{23} - ρ_{14}](t) and [ρ_{23} - ρ_{14}](t-δ) in the upper panel. The storage term in the LHS of equation (16) and the advective flux divergence, surface flux and dissipation terms in the RHS of equation (16) are shown in the lower panel. In this case, α, q and k_o are set to 2.0, 0.1 and 0.2, respectively, and the time delay δ is set to 20.

At (A), the density difference (ρ_{23} - ρ_{14}) is at the statistical equilibrium point of about 0.2. However, the advective flux divergence is minimized because the meridional transport, which is proportional to [ρ_{23} - ρ_{14}](t-δ), is very small at this point. Since the dissipation is also very small, the sum of the advective flux divergence and dissipation cannot balance the surface flux. Therefore, the density difference increases after this point. Between (A) and (B), the sum of the advective flux divergence and the dissipation is still smaller than the surface flux, thus the density difference (ρ_{23} - ρ_{14}) increases from its equilibrium to the maximum. Therefore, (A)-(B)

is a positive feedback period. At (B), the advective flux divergence is still weak, but the dissipation is at its maximum because the density difference (ρ_{23} - ρ_{14}) is maximized at this point. The sum of advective flux divergence and dissipation exactly cancel out the surface flux terminating the increase of the density difference. Therefore, the positive feedback ends at this point. Between (B) and (C), the advective flux divergence increases very rapidly. The sum of advective flux divergence and dissipation is now larger than the surface flux, and thus the density difference (ρ_{23} - ρ_{14}) swings back toward the statistical equilibrium point. Therefore, (B)-(C) is a negative feedback period.

At (C), the density difference (ρ_{23} - ρ_{14}) is once again at its statistical equilibrium point. However, the advective flux divergence is maximized and is much larger than the surface flux. Therefore, the density difference should further decrease beyond this point. It is interesting to note that both the meridional transport and the density difference are at their average values at this point, but the advective flux divergence is at its maximum. This is because if two signals are out-of-phase, their multiplication is maximized at crossing points. Imagine two functions that are out-of-phase, such as $A=cos(x)$ and $B=cos(x-\pi/2)$. The multiplication of the two functions will be always negative and the maximum is 0 at $x=n\pi/2$ where n is an integer value.

Between (C) and (D), the meridional transport increases, but the density difference is very small, thus the advective flux divergence decreases. Nevertheless, the advective flux divergence is still larger than the surface flux. Therefore, the density difference further decreases beyond its equilibrium value. This is a positive feedback period. At (D), the density difference is at its minimum. The sum of advective flux divergence and dissipation exactly cancel out the surface flux terminating the decrease of the density difference. Therefore, the positive feedback ends at this point. Between (D) and (E), the advective flux divergence decreases. Since the surface flux

is now larger than the advective flux divergence, the density difference (ρ_{23} - ρ_{14}) swings back from its minimum toward the equilibrium value. Therefore, (D)-(E) is a negative feedback period. At (E), the cycle restarts as in (A).

In summary, the delayed advective oscillator is maintained by alternating actions of amplification (i.e., positive feedback) and stabilization (i.e., negative feedback) through the oscillation of advective flux divergence. In one cycle of the delayed advective oscillator, there are two periods of amplification separated by two periods of stabilization. The first amplification occurs when the meridional density difference increases beyond the equilibrium point because the surface flux wins the competition with the advective flux divergence. The second amplification occurs when the meridional density difference decreases beyond the equilibrium point because the advective flux divergence becomes larger than the surface flux. During the stabilization periods, the density difference swings back from either its minimum or maximum point toward the equilibrium point through the competing effects of the surface flux and advective flux divergence.

To have an idea about the actual time scale of the delayed advective oscillator, let us consider typical parameter values for the North Atlantic: L_x = 5×10^6m; L_y=2.0×10^6m; g' = 1×10^{-2}m s^{-1}; f_o = 10^{-4} s^{-1}; β = 2×10^{-11} m^{-1} s^{-1}; and H = 2000m. The basin-crossing time can be estimate by L_x/c, where c (= $g'H\beta/(2f_o^2)$) is the long baroclinic Rossby wave speed. It is about 8 years in this case. Assuming that about 2~3 cycles of the basin-crossing time are required for the adjustment of density-driven gyre, the delay time is about 16 ~ 24 years. Since the time scale, $2f_oL_y^2/(g'H)$ = 1.3 years, δ = 12 ~ 18 for the North Atlantic case. Then, the AMOC cycle is about 30 to 50 years because the period of delayed advective oscillator is about 2δ.

5. Impacts of external forcing

Now, the responses of delayed advective oscillator to low frequency external forcing patterns, such as freshwater flux into the high-latitude North Atlantic associated with deglaciation periods (or with the anthropogenic global warming), and to high frequency external forcing patterns, such as weather noise related to the North Atlantic Oscillation (NAO), are explored here. Three low-frequency forcing experiments are performed, i.e., (a) deglaciation (or anthropogenic global warming), (b) complete shutdown of AMOC during Heinrich events, and (c) a cooing in the high-latitude North Atlantic. For each experiment, the following form of fresh water flux is used only in the high-latitude (i.e., box-2):

$$q_2 = q + q_o \exp\left(\frac{t^* - 40}{20}\right)^2 , \qquad (17)$$

where $t^* = t/\delta$, and q_o is set to $-q/2$, $-2q$, and $q/2$ for the deglaciation experiment, Heinrich mode experiment, and high-latitude North Atlantic cooling experiment, respectively. Note that the surface flux in the low-latitude is kept constant.

Figure 4 shows that the AMOC may slow down due to the fresh water flux in the high-latitude, but recovery is quite fast. This result is consistent with the externally forced model simulations for the 21st century used in the Intergovernmental Panel for Climate Change - 4th Assessment report (IPCC-AR4). An interesting point is that the amplitude of the delayed advective oscillator is reduced substantially and its recovery is extremely slow. As shown in the second panel of Figure 4, the AMOC can completely shut down if the surface flux becomes identical in the low- and high-latitude boxes. The AMOC recovers quickly when the external forcing is removed. However, the delayed advective oscillator is completely disrupted. The high-latitude North Atlantic cooling has a minor impact on the AMOC strength as shown in the third

panel of Figure 4. However, the delayed advective oscillator is weakened and slowly recovers when the external forcing is removed.

Next, the impact of high frequency forcing on the delayed advective oscillator is explored. It is widely believed that the high frequency portion of NAO originates from weather noise. Nevertheless, the NAO has a coherent spatial structure with a dipole-like meridional pattern of the sea level pressure. Due to this coherent spatial pattern, if the high-latitude is cooled, the mid-latitude is warmed, and vice versa. Therefore, the high frequency forcing of NAO is represented here as a random noise surface flux with anti-symmetric meridional pattern; that is, the sine of random forcing is opposite in the two latitudes boxes but with the same amplitude. Note that the random noise forcing does not produce a net surface flux into or out of the system. The amplitude of the random forcing is set to $q/2$.

Figure 5 shows the model solutions (a) with and (b) without the random forcing, and (c) with both the low- and high-frequency forcing for α=1.2, q=0.1, k_o=0.2, and δ=20. In the last case, the low frequency forcing is added only in the high-latitude (i.e., box-2) using the equation (17) with $q_o = -1.5q$. As shown in the mid panel, the delayed advection oscillation is damped out without the weather noise for given parameter values. Interestingly, if the weather noise is introduced, the delayed advective oscillator with the period of ~2δ can sustain its amplitude of up to 36% of the mean. It is also interesting to note that the solution with the weather noise forcing contains a very low-frequency variation on the order of 10~30 times the delayed advective oscillation period. Using realistic parameter values for the North Atlantic, it amounts to the centennial time scale. Figure 5(c) shows that even when the external forcing is large enough to nearly shutdown the AMOC, the weather noise can invigorate the delayed advective oscillator once the external forcing is removed.

In summary, the AMOC is remarkably stable because it always swings back to its original state once an external forcing is removed. This is true even when the AMOC is completely shut down as in during Heinrich events. The delayed advective oscillator is, on the other hand, very fragile. If an external forcing is large enough, it can virtually wipe out the delayed advective oscillator. The recovery of the delayed advective oscillator is extremely sluggish. However, that these are characteristics of the delayed advective oscillator in its pure form. If weather noise forcing is added to the system, the behavior of the delayed advective oscillator is drastically changed. In particular, relatively large amplitude of weather noise can sustain an active delayed advective oscillation of an otherwise stable system. The AMOC can still shut down if the external forcing is large enough. However, the weather noise can quickly invigorate the delayed advective oscillator once the external forcing is removed. Finally the weather noise can also produces a very low-frequency fluctuation at the centennial time scale.

An important question is why the delayed advective oscillator is excited by weather noise. The simple stochastic climate model of Hesselmann (1976) provides a plausible explanation for this question. It is well known since Hesselmann (1976) that a random noise atmospheric forcing produces a red noise spectrum of ocean temperature via ocean memory. If this theory is applied to the four-box model, it means that a random surface forcing produces large amplitude of signal in the meridional density difference field, (ρ_{23} - ρ_{14}), at low frequencies including at the frequency of delayed advective oscillator, $\omega \sim 0.5\delta^{-1}$. Therefore, the delayed advective oscillation can be excited and maintained by weather noise even if it is a damped oscillation as shown in Figure 5(a).

6. Linear stability analysis

To better understand how the four parameters, α, q, k_o, and δ influence the delayed advective oscillator, a linear stability analysis of the nonlinear system of equations (7)-(10) is performed. First, the stationary solutions with δ=0 are obtained by numerically integrating the equations (7)-(10). Replacing the solutions with the sum of stationary solution and perturbation, and retaining only the linear terms can derive the perturbation equations (not shown). Seeking solutions of the form $\rho_k' = c_k \exp(\sigma t)$ with k=1, 2, 3 and 4, and $\sigma = \sigma_r + i\sigma_i$, a matrix equation can be derived:

$$\begin{bmatrix} a_{11} & a_{12} & a_{13} & a_{14} \\ a_{21} & a_{22} & a_{23} & a_{24} \\ a_{31} & a_{32} & a_{33} & a_{34} \\ a_{41} & a_{42} & a_{43} & a_{44} \end{bmatrix} \cdot \begin{bmatrix} c_1 \\ c_2 \\ c_3 \\ c_4 \end{bmatrix} = 0 . \tag{18}$$

The determinant of the matrix **A** must vanish in order for nontrivial eigenfunctions to exist: this yields an equation for the calculation of the complex eigenvalue σ for chosen values of α, δ, k_o and q. Since the matrix **A** contains the eigenvalue σ and its exponential form, $\exp(-\sigma\delta)$, an iterative Muller's method is used to obtain the eigenvalue σ.

Figure 6 shows the neutral curves (a) on the α-δ plane for q=0.1 and k_o=0.2, (b) on the k_o-δ plane for α=2.0 and q=0.1, and (c) on the q-δ plane for α=2.0 and k_o=0.2. For a given value of δ, increasing α and decreasing k_o destabilize the system. These results are not surprising since α is proportional to the meridional volume transport, which provides the positive feedback required to maintain the delayed advective oscillation, thus serves as a growth rate, and k_o serves as a damping rate. It is important to note that the neutral curve on the q-δ plane is not monotonic. For a given value of δ, the system is unstable only when q is within a certain range. This strongly supports an idea that the delayed advective oscillator exists via a delicate balance of various

terms, and also nicely explains why the delayed advective oscillator (in its pure form) is so fragile under the impacts of external forcing as shown in Figure 4.

7. Discussions

Perhaps, the four-box model presented here is the simplest dynamic model for explaining the results of general circulation models that produce the multidecadal oscillation of AMOC (e.g., Delworth et al. 1993; Knight et al. 2005). Despite the overly simplified nature of the model, this minimum complexity model describes the important mechanism of the delayed advective oscillator, which appears to be the key for improving our understanding of the AMOC and its multidecadal oscillation. However, there are many remaining questions to be explored. One important issue is to estimate the realistic values for α, k_o, and δ for the AMOC. A related question is if the AMOC is an unstable regime or is subject to a damped oscillation, which requires weather noise to maintain its multidecadal oscillation. These are apparently important issues, and should be the subjects of future studies.

The delayed advective oscillator can be compared to the delayed action oscillator for ENSO (Suarez and Schopf 1988) because the key element in both cases is the oceanic Rossby wave transit effects. However, there is an important distinction between the two oscillation mechanisms. In the case of delayed action oscillator, the equatorial oceanic Rossby wave transit effects provide a *negative* delayed feedback to an otherwise linearly amplifying system. In the case of the delayed advective oscillator, the advective flux divergence delayed by the oceanic Rossby wave transit effects provide both the *negative* and *positive* feedbacks required to maintain the oscillation.

Finally, the four-box model can be modified or expanded for various thought experiments. For instance, the density equations (7)-(10) can be readily expanded to two sets of equations for salinity and temperature equations to explore the effects of external heat flux and freshwater flux, separately. The model domain can be also expanded to include the South Atlantic and Southern Ocean. The four-box model with a weather noise forcing may be also used to improve our understanding of fundamental issues such as decadal predictability of the AMOC.

References

Delworth, T., S. Manabe, and R. Stouffer, 1993: Interdecadal Variations of the Thermohaline Circulation in a Coupled Ocean-Atmosphere Model. *J. Climate*, 6, 1993–201

Hasselmann, K., 1976: Stochastic climate models, Part I, Theory. *Tellus*, 28, 473-485.

Killworth, P. D., 1985: A two-level wind and buoyancy driven thermocline model. *J. Phys. Oceanogr*. **15**, *1414-1432*.

Knight, J. R., R. J. Allan, C. K. Folland, M. Vellinga, and M. E. Mann, 2005: A signature of persistent natural thermohaline circulation cycles in observed climate, *Geophys. Res. Lett.*, 32, L20708, doi:10.1029/2005GL024233.

Suarez, M. J., and P. S. Schopf, 1988: A delayed action oscillator for ENSO. *J. Atmos. Sci*., 3283-3287.

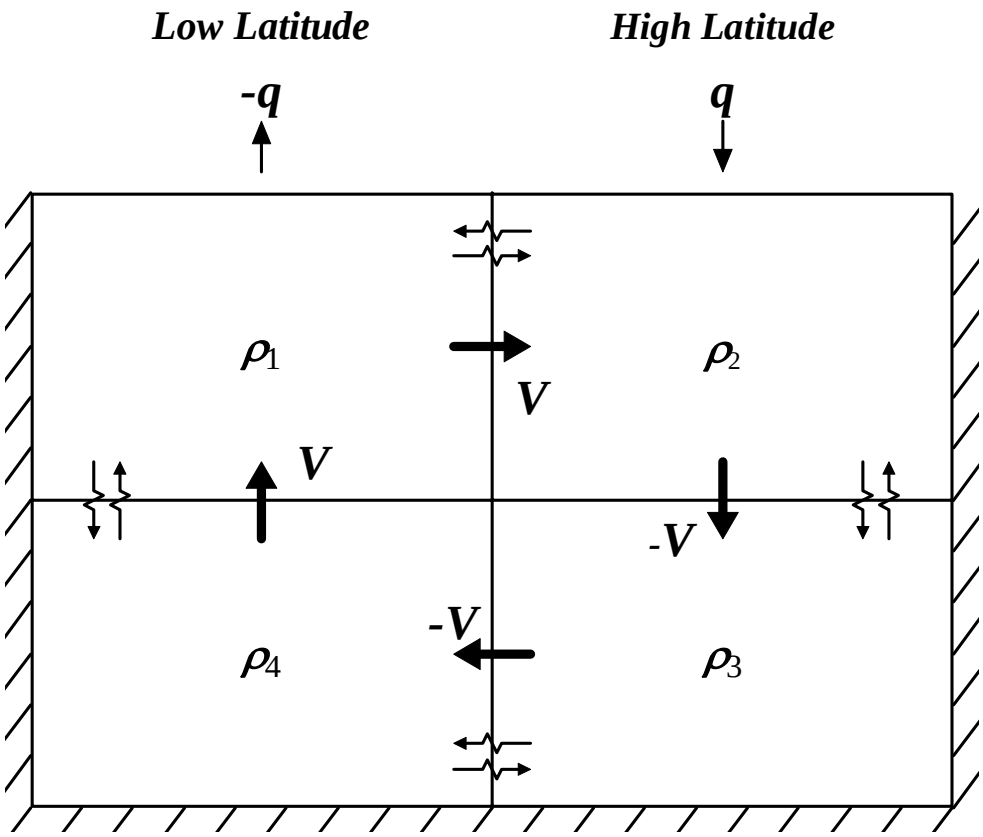

Figure 1. The North Atlantic Ocean is simplified with four boxes. Since the meridional density gradient is always positive, the volume transport (per unit volume) V is always northward in the upper layer and southward in the lower layer. ρ_1, ρ_2, ρ_3 and ρ_4 are densities of the upper low-latitude box, upper high-latitude box, lower high-latitude box, and lower low-latitude box, respectively. q is density flux into the upper high-latitude box (or out of the upper low-latitude box).

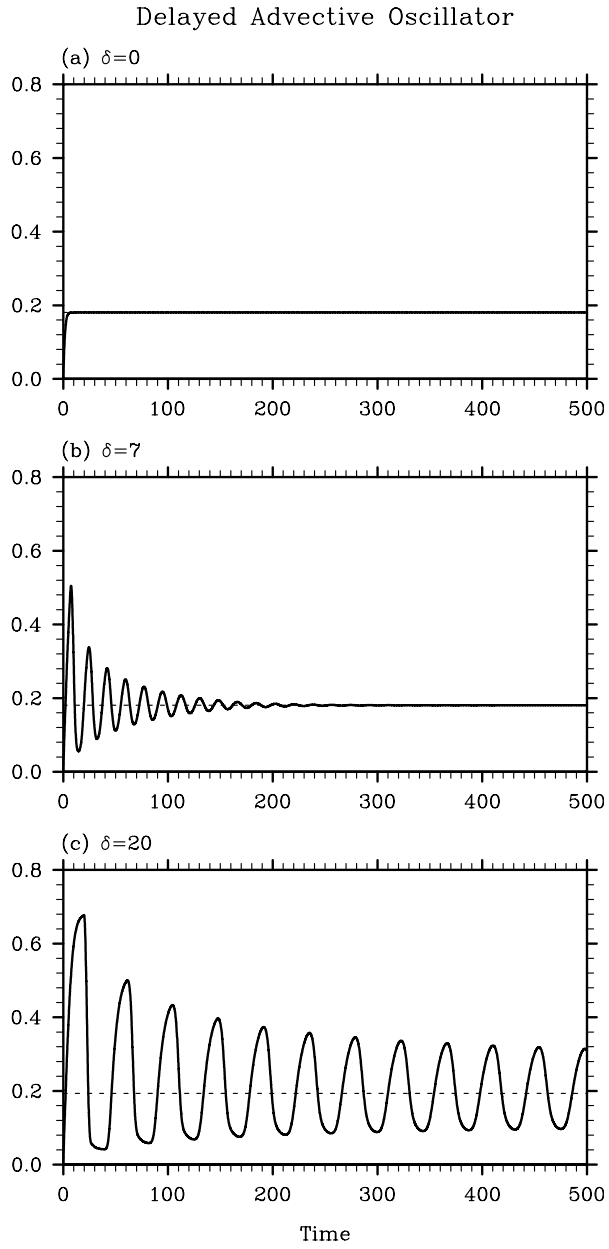

Figure 2. Three model solutions, (ρ_{23} - ρ_{14}), for (a) $\delta = 0$, (b) $\delta = 7$ and (c) $\delta = 20$. α, q and k_o are set to 2.0, 0.1, and 0.2, respectively. The dashed lines are the statistical equilibrium values. For small values of δ, the solution achieves a stable state. For a larger value of δ, on the other hand, the solution oscillates with a period of about twice the delay.

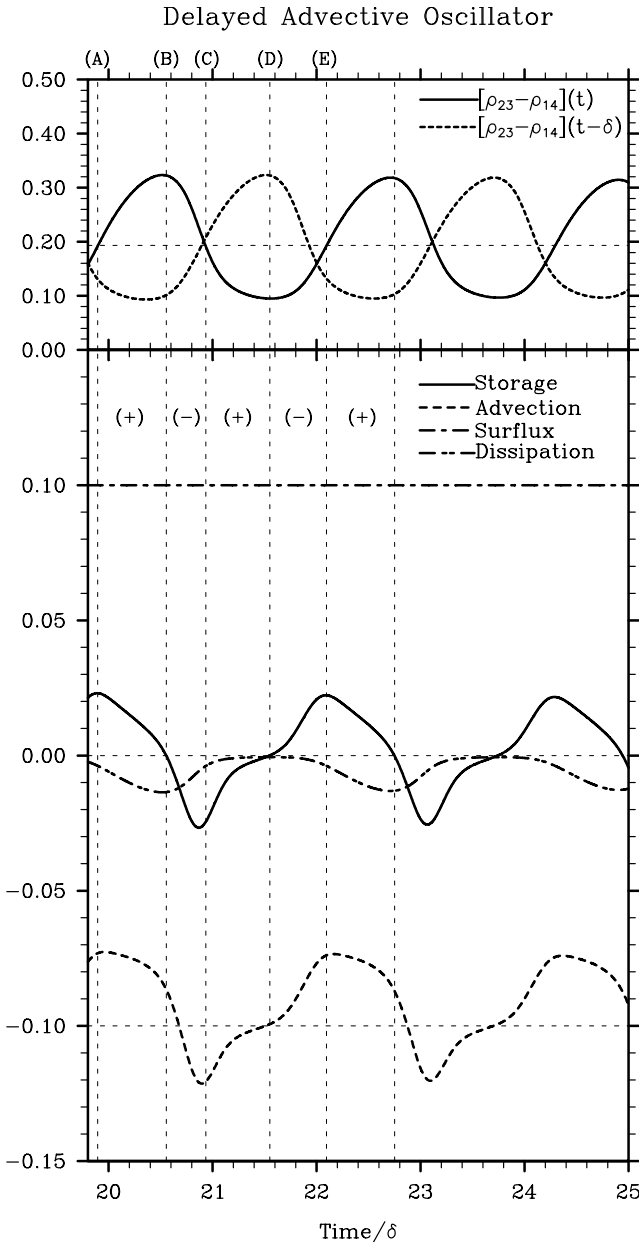

Figure 3. The model solutions [ρ_{23} - ρ_{14}](t) and [ρ_{23} - ρ_{14}](t-δ) are shown in the upper panel. The storage term in the LHS of equation (11) and the advective flux divergence, surface flux and dissipation terms in the RHS of equation (11) are shown in the lower panel. δ, α, q and k_o are set to 20, 2.0, 0.1, and 0.2, respectively. The symbols (+) and (-) represent the period of positive and negative feedback, respectively. See text for the descriptions of density budgets at (A), (B), (C), (D) and (E).

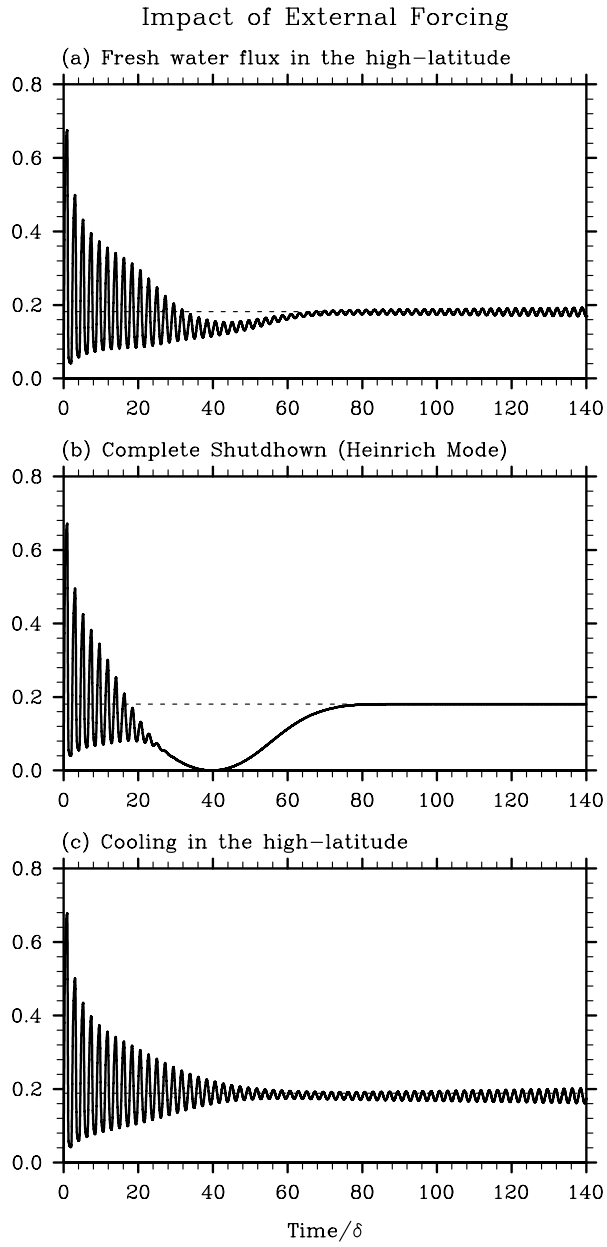

Figure 4. The responses of the delayed advective oscillator to the external forcing of (a) deglaciation (or anthropogenic global warming), (b) complete shutdown of AMOC during Heinrich events, and (c) a cooing in the high-latitude North Atlantic. The amplitude of the external forcing q_o is set to q/2, -2q, and q/2 for (a), (b) and (c), respectively. δ, α, q and k_o are set to 20, 2.0, 0.1, and 0.2, respectively.

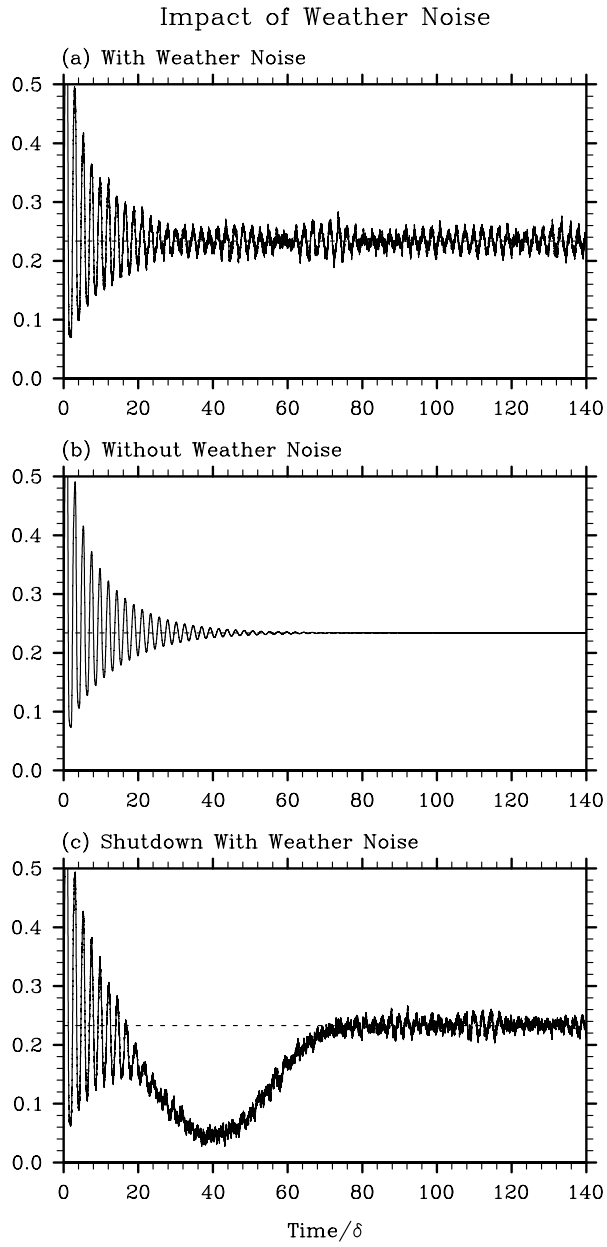

Figure 5. The behavior of delayed advective oscillator (a) with and (b) without the random noise forcing, and for (c) a case with both the low- and high-frequency forcing. The amplitude of the random forcing is set to $q/2$ for (a) and (c). For (c), q_o = -1.5q. δ, α, q and k_o are set to 20, 1.2, 0.1, and 0.2, respectively.

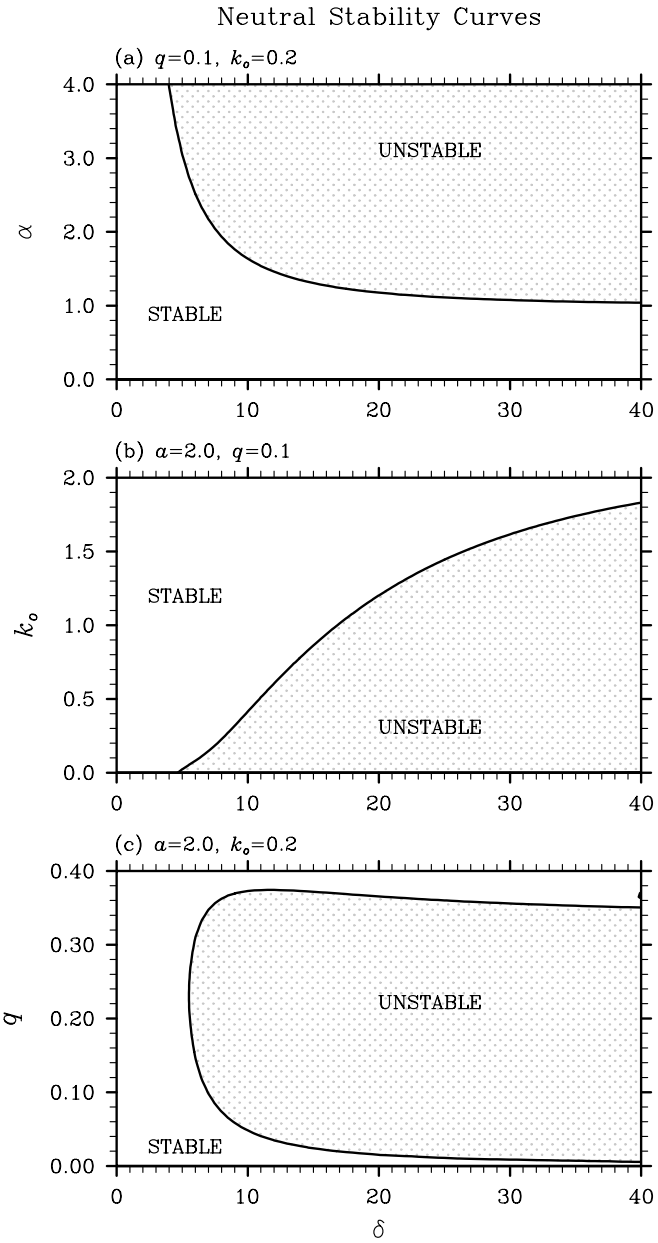

Figure 6. Neutral stability curves (a) on the α-δ plane for q=0.1 and k_o=0.2, (b) on the k_o-δ plane for α=2.0 and q=0.1, and (c) on the q-δ plane for α=2.0 and k_o=0.2.